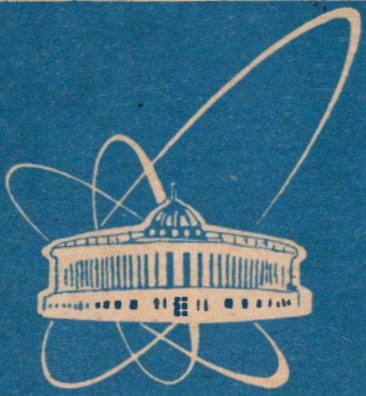

ОБЪЕДИНЕННЫЙ
ИНСТИТУТ
ЯДЕРНЫХ
ИССЛЕДОВАНИЙ

Дубна



E15-97-9

V.V.Filchenkov

# TRANSITION PROCESSES IN THE NOVEL METHOD OF THE MUON CATALYSIS INVESTIGATION

Submitted to «Hyperfine Interaction»

1997

## I. Introduction

The experimental program of the investigations of the $d+t$ muon catalyzed fusion (MCF) reactions is now realized in a the frame of the large international project TRITON aimed to measure the characteristics of the d+t fusion cycle in the double D/T and the triple H/D/T mixture of high density (up to the liquid hydrogen density, LHD). Simplified scheme of the process is shown in Fig. 1.

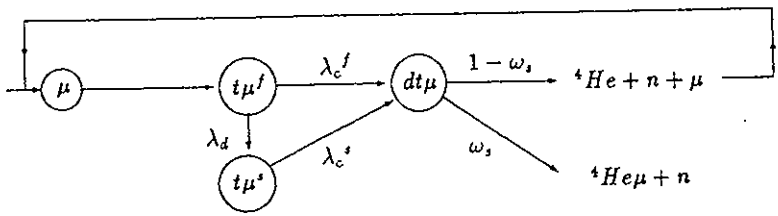


Figure 1: Simplified scheme of the muon catalysis process.

As follows from theory and experiment, the "effective" sticking probability of muon to helium (taking into account the muon sticking in the $d+d$ and $t+t$ accompanied reactions) is to be $\omega \simeq 0.005$. Under the optimal experimental conditions (high density and high tritium concentration) the value of the cycling rate $\lambda_c{}^f$ can achieve $100 - 150\,\mu s^{-1}$ that is large compared with the muon decay rate $\lambda_0 = 0.455\,\mu s^{-1}$. Thus the yield of the $d+t$ fusion reactions can be $Y_n \simeq 150\,n/\mu$.

The experimental method is characterized by two principal features providing the direct measurement of Y and $\omega$ [1], [2], [3]:

1. The time spectrum of the last detected neutron relative to muon decay ($t_e - t_n$ spectrum) and the neutron multiplicity (number of detected neutrons, $k$, per muon) $N(k)$ distribution are suggested to be measured. Note that only time spectra of all

detected neutrons have been previously measured and analyzed by other authors.
2. Charge distributions of the neutron detector signal are measured instead of the distributions of the number of events to eliminate the experimental spectrum distortions due to the *pile up* effects . Flashes ADC are used for this.

Methods of the experimental data presentation and analysis were considered in our previous paper [4]. The steady state case was considered in it, when only one rate of the d-t fusion cycle ($\lambda_c$) together with $\omega$ determine the muon catalysis intensity. Now we involve into consideration the fast transition processes. The most important of them are connected with the "hot" mu-atom ($t\mu^f$) thermalization stage, from the initial energy $E_0 \sim 1 - 10\, eV$ to the thermal one $E_{th} \sim 10^{-2} - 10^{-3}\, eV$, during which it meets the very high intensive resonances in the $dt\mu$-molecule formation [5], [6].

As follows from the theory, the value of the $dt\mu$-formation rate at the fast stage can achieve $(10^9 \cdot - 10^{10}) \cdot \phi\, s^{-1}$, while for the thermal mu-atoms ($t\mu^s$) it is $\sim 10^8 \cdot \phi\, s^{-1}$. (Here $\phi$ is the hydrogen density relative to LHD.) The deceleration rate is expected to be $\lambda_d \sim \phi \cdot 10^9\, s^{-1}$. Hence, in spite of the very short part of the $t\mu$-atom history it can essentially influence the MCF characteristics.

The goal of the present paper is to explore how the presence of the fast MCF stage affects the character of the $t_e - t_n$ and $N(k)$ distributions, whose form have been obtained by us [2], [3] in the one state approximation. Again, as in our previous paper [4], we shall follow the line of an "effective" analysis aimed to obtain the main "macroscopic" parameters: neutron yield per muon ($Y_n$), effective sticking ($\omega$) and cycling rate. The "microscopic" characteristics, such as the $dt\mu$-molecule formation rate, can be extracted from them in the subsequent detailed analysis of the data measured at different experimental conditions.

## II. Kinetics

Kinetics of the MCF cycle was considered in many works. Detailed description of the d-d cycle kinetics involving the spin flip transitions was made in [7] and in the following papers by solving the differential equations for the corresponding populations of mu-atoms as functions of time. Kinetics of the d-t cycle was first studied in [8]. Most of the authors dealt with the time distribution of all detected neutrons independent of the neutron detection efficiency $\epsilon$. Time distributions of the first, second and subsequent neutrons detected with efficiency $\epsilon$ were first obtained in [9] for the steady state case (one state approximation). The spin flip transition process for the d-d cycle with account of the efficiency $\epsilon$ was considered in [10].

The effect of the epithermal ("hot") mu-atoms in the measured neutron time distributions manifests itself in appearance of the "fast" component (spike) and modification of the parameters for the slow component (*steady state*) compared with the pure one state case. This was observed experimentally in measurement of time spectra of all detected neutrons and analyzed in a few papers (see, for example, [11], [12] and [13]). As follows from [12], the MCF at the fast stage results in a 10-40 % increase of the total neutron yield.

To estimate the effect of the thermalization stage we consider the simplest model in which mu-atoms are formed in the state characterized by the deceleration rate $\lambda_d$ and by a larger cycling rate $\lambda_c{}^f$ than $\lambda_c{}^s$ for the steady state when thermalization takes place (see Fig. 1). The following differential equations correspond to the scheme



of the processes shown in Fig. 1:

$$dn_f/dt = -(\lambda_0 + \lambda_d + \lambda_c{}^f) \cdot n_f(t) + (1-\omega)\lambda_c{}^s \cdot n_s(t) + (1-\omega)\lambda_c{}^f \cdot n_f(t)$$

$$dn_s/dt = -(\lambda_0 + \lambda_c{}^s) \cdot n_s(t) + \lambda_d \cdot n_f(t).$$

Here $n_f$ and $n_s$ are the populations of the fast and thermalized mu-atoms as functions of time, other notations can be seen in Fig. 1. The time distribution of all detected neutrons has the form

$$dN/dt = \epsilon \cdot (\lambda_c{}^f \cdot n_f + \lambda_c{}^s \cdot n_s).$$

From the mathematical point of view the solution of this task is just similar to the one obtained in [10] with change of the initial populations of mu-atom states. In the present case they are $n_f(t=0) = 1$ and $n_s(t=0) = 0$. Using the results of [10], we find that both for all detected neutrons and for the first detected ones the time distribution has the form

$$dN/dt = \epsilon \cdot [A_f \cdot exp(-\gamma_f t) + A_s \cdot exp(-\gamma_s t)], \qquad (1)$$

where the first term corresponds to the fast transition process and the second one to the steady state stage. The slopes of exponents are

$$\gamma_f \simeq \lambda_0 + \lambda_d + \lambda_c{}^s + \alpha\lambda_c{}^f,\ \gamma_s \simeq \lambda_0 + \alpha\lambda_c{}^s(\lambda_d + \lambda_c{}^f)/(\lambda_d + \lambda_c{}^s + \alpha\lambda_c{}^f),$$

where $\alpha = \omega$ for all detected neutrons and $\alpha = \epsilon + \omega - \epsilon\omega$ for the first detected ones. Contrary to the one state approximation, where $A_s = \lambda_c$ and $\gamma_s = \lambda_0 + \alpha\lambda_c$, now the exponent amplitudes and slopes are functions of all parameters $\lambda_d$, $\lambda_c{}^f$ and $\lambda_c{}^s$. The amplitude $A_s$ for all detected neutrons will be also called the steady state cycling rate $\lambda_{ss}$.

Exact parameters of expression (1) were calculated by a special code. To check the calculations we use the Monte-Carlo program in which all processes shown in Fig. 1 were involved into consideration with these rates set as input parameters. Appropriate distributions were accumulated in the output of the program and then fitted by expression (1). The parameters obtained were compared with the exact solutions.

Table 1. Parameters of the neutron time distributions (1) calculated for the values (2), $\omega = 0.005$ and $\epsilon = 0.3$.

| Parameter | All detected neutrons | | First detected neutrons | |
|---|---|---|---|---|
| | Exact solution, ($\alpha = 0.005$) | Monte-Carlo | Exact solution, ($\alpha = 0.3035$) | Monte-Carlo |
| $\gamma_f$ | 40.5 | $41.5 \pm 2.3$ | 43.0 | $42.8 \pm 1.6$ |
| $\gamma_s$ | 0.517 | $0.517 \pm 0.001$ | 4.03 | $4.04 \pm .01$ |
| $A_f/A_s$ | 0.603 | $0.629 \pm 0.025$ | 0.817 | $0.829 \pm .017$ |

The example of comparison is given in Table 1. Here we used the values

$$\lambda_d = 30\, \mu s^{-1},\ \lambda_c{}^f = 20\, \mu s^{-1},\ \lambda_c{}^s = 10\, \mu s^{-1}. \qquad (2)$$

This situation could be hardly realized in experiment (really $\lambda_d$, $\lambda_c{}^f >> \lambda_c{}^s$) but allows one to effectively estimate the effects considered. (Note that the values (2) are the effective ones, i.e. multiplied by the appropriate values of relative hydrogen density and hydrogen isotope concentrations.) As is seen from the table, there is good agreement between the calculated values and the ones obtained with the Monte-Carlo simulations, which allows confidence in the correct consideration.

The distribution of the last detected neutron relative to muon decay ($t_n - t_e$ spectrum) is of special interest in our experiment [1], [3]. The formula for this spectrum with the finite neutron detection efficiency taken into account was first presented in [2] for the one state approximation. It is a sum of two exponents

$$dN/dt = \epsilon A_s \cdot exp(-\gamma_s t) + A_0 \cdot exp(-\lambda_0 t),$$

where the ratio $A_0/A_s$ is

$$A_0/A_s = \omega/\epsilon(1-\omega). \qquad (3)$$

If the transition process is involved into consideration, then an expression for the $t_n - t_e$ distribution becomes a sum of three exponents

$$dN/dt = \epsilon A_f \cdot exp(-\gamma_f t) + \epsilon A_s \cdot exp(-\gamma_s t) + A_0 \cdot exp(-\lambda_0 t), \qquad (4)$$

where the values of $\gamma_f$ and $\gamma_s$ are just the same as for the first detected neutrons. The origin of each term of Eq. 3 is the following. The first two exponents correspond to muon decay from the states of the "hot" and thermalized $t\mu$-atoms respectively and the third one is due to the muon sticking to helium. In this case

$$A_0/A_s = (\gamma_s - \lambda_0)/\epsilon A_s(1-\omega) - 1 - A_f(\gamma_s - \lambda_0)/A_s(\gamma_f - \lambda_0). \qquad (5)$$

In the absence of transitions, when $A_f = 0$, $A_s = \lambda_c$, $\gamma_s = \lambda_0 + \lambda_c(\epsilon + \omega - \epsilon\omega)$, expression (5) coincides with (3). Again we obtained the exact values for the parameters of Eq. 4 and compared them with the ones obtained from the analysis of the simulated distributions. To compare two variants - with and without transitions - (and check the program) the calculations were also done with $\lambda_d \neq 0$ and $\lambda_c{}^f = \lambda_c{}^s$. An example of such comparison is presented in Table 2, and the appropriate time distributions are shown in Fig. 2.

Table 2. Parameters of time distribution (4) of the last detected neutrons relative to muon decay obtained for $\omega = 0.005$, $\epsilon = 0.3$, $\lambda_d = 100\,\mu s^{-1}$ and $\lambda_c{}^s = 10\,\mu s^{-1}$. The two states variant corresponds to $\lambda_c{}^f = 50\,\mu s^{-1}$ and the one state one to $\lambda_c{}^f = \lambda_c{}^s = 10\,\mu s^{-1}$.

| Parameters of expression (4) | Output values | | | |
|---|---|---|---|---|
| | Two states | | One state | |
| | Exact solution, | Monte-Carlo | Exact solution, | Monte-Carlo |
| $\gamma_f$, $\mu s^{-1}$ | 122 | $129 \pm 12$ | | |
| $\gamma_s$, $\mu s^{-1}$ | 4.20 | $4.21 \pm 0.01$ | 3.49 | $3.48 \pm 0.01$ |
| $A_f/A_s$ | 0.108 | $0.122 \pm 0.012$ | | |
| $A_0/A_s$ | 0.0185 | $0.0184 \pm 0.0002$ | 0.0167 | $0.0165 \pm 0.0002$ |



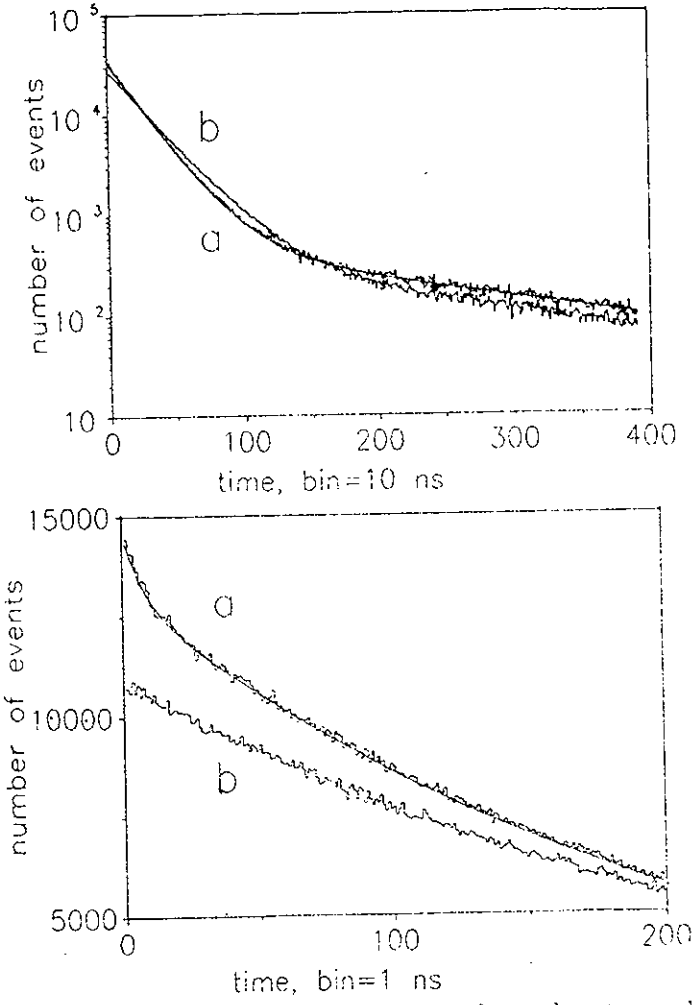


Figure 2: Simulated time distributions of the last detected neutrons relative to muon decay. The histograms represent the Monte-Carlo calculations and curve is the fitting function (4). The values $\lambda_d = 100\,\mu s^{-1}$ and $\lambda_c{}^s = 10\,\mu s^{-1}$ were used in calculations. Variant (a) corresponds to $\lambda_c{}^f = 50\,\mu s^{-1}$ and variant (b) was calculated with $\lambda_c{}^f = \lambda_c{}^s = 10\,\mu s^{-1}$ (one state approximation.)

All three exponents are clearly shown in this figure for the specially chosen not very large rates (they correspond to the "approximate real" case for $\phi = 0.1$) and special scaling of the pictures.

As is seen from Table 2, the ratio $A_0/A_s$ is changed compared with the "original" value $A_0/A_s = \omega/\epsilon = 0.0167$. Sensitivity of this ratio to the value of $\lambda_c{}^f$ under fixed value $\lambda_c{}^s = 10\,\mu s^{-1}$ is demonstrated in Fig. 3, in which the fit results are given together with the exact calculations.

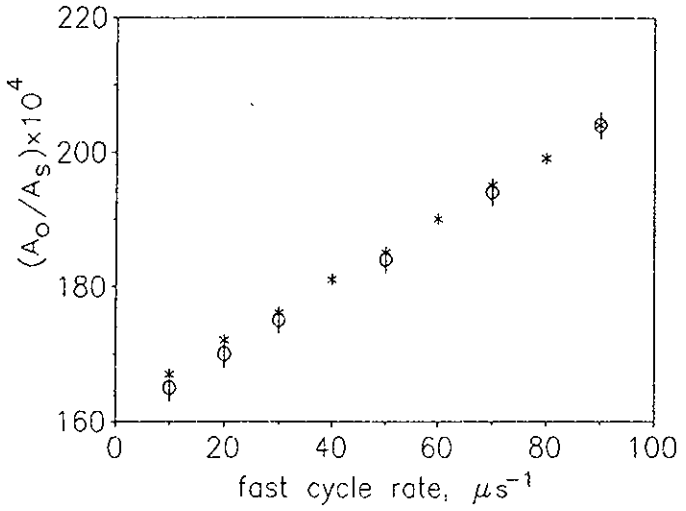


Figure 3: Ratio of the "$\lambda_0$ - component" amplitude to the steady state one of the $t_e - t_n$ - spectrum calculated for the MCF parameters presented in Table 2. Stars show the exact solutions, circles correspond to the fit of simulated distributions.

Thus, as follows from the consideration of the problem, to directly obtain the value of the muon sticking probability from the $t_e - t_n$ - spectrum we must know the parameters of the very short-lived component of the neutron time distribution which is rather difficult to observe in an experiment.

Now let us consider the neutron multiplicity distribution $N(k)$ for some definite time interval $T$ where muon does not disappear. As follows from [2], this distribution can be represented as a sum of two terms. One of them, $f(k)$, corresponds to "sticked" events and the other one, $g(k;m)$, is the Gaussian (Poisson):

$$N(k) = N_1 \cdot [f(k) + (1-\xi)^m \cdot g(k;m)]\,. \qquad (6)$$

Here $N_1$ is the total number of the first detected neutrons in the time interval T (the sum of $N(k)$). The transition processes neglected (one cycling rate approximation), the mean value of the Gaussian is

$$m = \epsilon\lambda_c T\,. \qquad (7)$$



Under the condition $m >> 1$ the distribution of the "sticked" events is described by the formula

$$f(k) = y_{k-1} - y_k = y_1 \cdot [1 - y_1 \cdot (1-\omega)] \cdot [y_1 \cdot (1-\omega)]^{k-1},$$

where $y_k$ is the relative yield of the $k$-th detected neutrons, $\xi = \omega/\epsilon_n$. It is important, that for the chosen selection criteria $t_e > T$ $y_1$ does not depend on $\lambda_c$: $y_1^{-1} = 1 + \xi - \omega$. Analysis of the $N(k)$ distribution makes it possible to find the values both of $m$ and $\omega/\epsilon$.

The thermalization stage with a high cycling rate gives rise to an increase in the value of $m$. But the function $f(k)$ does not depend on the cycling rate, therefore it does not change its form while the thermalization stage is taken into account. As the mean value of the peak and its weight $(1-\omega/\epsilon)^m$. can be determined independently, $\omega/\epsilon$ could be reliably found without any assumptions of the fast stage parameters.

Our aim is to check this and simultaneously to try to interpret the peak shift. As previously, we checked our estimations by their comparison with the Monte-Carlo calculations.

The consideration of the problem shows that $m$ is defined by the expression

$$m = \epsilon\lambda_c{}^s T \cdot (1 + \delta m), \quad \delta m = (\lambda_c{}^f - \lambda_c{}^s)/(\lambda_d + \lambda_c{}^s)\,. \qquad (8)$$

The values of $m$ obtained with (8) and found from the fit of the Monte-Carlo distributions are given in Table 3. The one-state variant ($\lambda_c{}^s = \lambda_c{}^f = 100\,\mu^{-1}$) is also presented to show the change in the value of $m$ with the fast stage parameters.

Table 3. Parameters of the neutron multiplicity distributions calculated with (8) and obtained from the analysis of the Monte-Carlo distributions for $\lambda_c{}^s = 100\,\mu s^{-1}$, $T = 2\,\mu s$, $\omega = 0.005$ and $\epsilon = 0.3$.

| Values used in calculations | | Parameters of expression (6) | | | |
|---|---|---|---|---|---|
| | | $\xi$ | | $m$ | |
| $\lambda_d$, $\mu s^{-1}$ | $\lambda_c{}^f$ $\mu s^{-1}$ | Exact solution | Monte-Carlo | Exact solution | Monte-Carlo |
| 300 | 100 | 0.0167 | 0.0171(2) | 60 | 59.7(2) |
| 300 | 300 | 0.0167 | 0.0168(3) | 90.0 | 89.3(5) |
| 600 | 300 | 0.0167 | 0.0172(4) | 77.1 | 76.2(4) |
| 1000 | 1000 | 0.0167 | 0.0167(2) | 109.1 | 109.0(3) |

As follows from Table 3, we can correctly explain modification of the neutron multiplicity distribution due to taking into account the fast cycling rate of the deceleration stage. Note that the values of $m$ coincide within 1% with the ones obtained with formulae (7) where $\lambda_c$ is the amplitude $A_s$ in expression (2) for all detected neutrons. It is a remarkable fact that the value of $\xi = \omega/\epsilon$ remains constant under any assumptions of the fast cycle parameters.

## III. Estimated results of measurements to be made with large neutron detector and FADC

In this section we apply our previous conclusions to the real situation:

1. As expected [5], [6], [14], in the D/T mixture of high density the rate of $t\mu$-atom deceleration and the fast cycling rate are $\lambda_d, \lambda_c{}^f \sim 10^3\,\mu s^{-1}$, which is much higher than $\lambda_c{}^s \sim 100\,\mu s^{-1}$. In this conditions it is very difficult to directly observe the prompt component in the neutron time spectra by our technique. The visible effect should be expected as a change in the steady state rate which manifests itself in increasing values of the neutron yield and in the steeper slope of the appropriate exponent:

$$Y \longrightarrow\simeq Y(1+\eta),\ \gamma_s \simeq \lambda_0 + \alpha\lambda_c{}^s \longrightarrow\simeq \lambda_0 + \alpha\lambda_c{}^s(1+\eta),$$

where $\eta \simeq \lambda_c{}^f/\lambda_d$ (recall that $\alpha = \omega$ for all detected neutron and $\alpha = \epsilon + \omega - \epsilon\omega$ for the first detected ones).

2. As in our previous paper [4], we simulated distributions taking into account the parameters of the measurements system including a neutron detector (ND) and flashes ADC. A specific feature of our ND [15] is a high detection efficiency. For $14MeV$ neutrons from the $d+t$ fusion reaction it is $\epsilon = 0.2 \div 0.3$. We took into account the recoil proton energy spectrum and the timing shape of the ND signal. FADC scan the ND signal with $100\,Mc$ strob pulse series with a random phase.

Monte-Carlo calculation programs allow the determination of the total charge $Q$ (the sum of amplitudes measured by FADC) and the total number of the detected neutrons $N_n$. The distributions calculated in the "charge mode" (with ND and FADC) were normalized to the unit charge $q = Q/N_n$. This makes possible their accurate comparison with the ones obtained in the "event mode". Below we present the main results.

Figure 4 shows the time distributions of all detected neutrons simulated on the assumption of one cycling rate (stars) and with taking the deceleration stage taking into account. For the latter case, the spectrum obtained in the "event mode" is presented as a histogram, the "charge mode" distribution is shown by circles. All spectra presented in Fig. 4 were obtained for the same number of muons $N_\mu = 10^4$. The values

$$\omega = 0.005,\ \epsilon = 0.3,\ \lambda_c{}^s = 100\,\mu s^{-1},\ \lambda_d = 1000\,\mu s^{-1} \qquad (9)$$

were used in calculations. The parameters found from the fit are given in Table 4.

As can be seen from Fig. 4, the "charge mode" distribution practically coincides with the appropriate "event mode" spectrum except for the initial channels, where ND and FADC are not able to reproduce the prompt spike. At the same time, as follows from the data of Table 4, the steady state rate is reproduced very well.

As we showed in our previous paper [4], the $t_e - t_n$ - distribution simulated in the one-state approximation with account of FADC is well fitted with the expression (4) for $A_f = 0$. Some shift in the value of $A_0/A_s$ was noted as compared with the expected value of $\omega/\epsilon$ for a long ND signal. In this case, very short component that is poorly resolved experimentally complicates determination of the ratio $\omega/\epsilon$. But the slope of the steady state exponent is correctly determined from the analysis of this distribution.



Table 4. Parameters of the time distributions of all detected neutrons presented in Fig. 4. The value of the neutron yield is related to the first $4\,\mu s$.

| Values used in calculations | | Parameters obtained | | | | |
|---|---|---|---|---|---|---|
| | | | | | $\gamma_s$ | |
| $\lambda_c{}^f$, $\mu s^{-1}$ | $\lambda_c{}^s$ $\mu s^{-1}$ | $N_n/N_\mu$ | $Q/N_n$ | $t_0$, $ns$ | Exact solution | Monte-Carlo |
| 1000 | 100 | 40.1 | 65.0 | 112.5(2) | 1.361 | 1.35(2) |
| 100 | 100 | 30.9 | 64.5 | 108.5(2) | 0.955 | 0.951(2) |

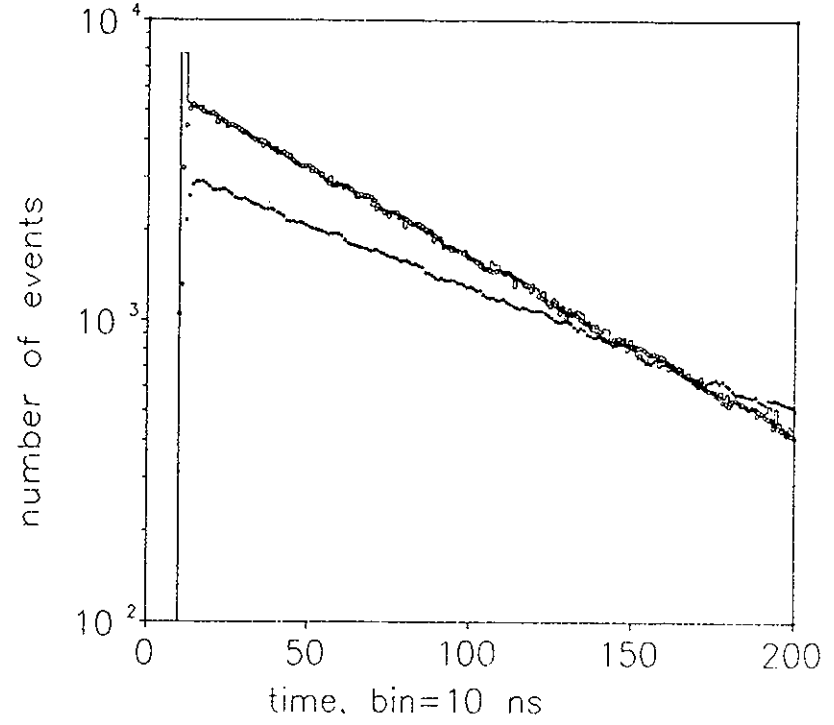


Figure 4: Simulated time distributions of all detected neutrons. The values (9) were used in calculations. The histogram and circles correspond to the case where the deceleration stage was taken into account ($\lambda_c{}^f = 1000\,\mu s^{-1}$, $\lambda_c{}^s = 100\,\mu s^{-1}$), the spectrum shown by stars is obtained for the one cycling rate approximation ($\lambda_c{}^f = \lambda_c{}^s = 100\,\mu s^{-1}$).

Figure 5 shows the neutron multiplicity distributions simulated with the values (9) in the "event mode" (histograms) and "charge mode" (circles). Histogram "a" corresponds to the one-state variant: $\lambda_c{}^f = \lambda_c{}^s = 100\,\mu s^{-1}$. Spectra "b" were calculated with $\lambda_c{}^f = 1000\,\mu s^{-1}$, $\lambda_c{}^s = 100\,\mu s^{-1}$.

To analyze the "charge mode" distribution we modified the formulae (6) to the form where the mean value of the Gaussian is $M = m \cdot q$:

$$N(k) = N_1 \cdot [f(k) + (1-\xi)^m \cdot g(k; M)] . \qquad (10)$$

Of course, for the normalized distribution the expected value of $q$ is $q = 1$ ($M = m$). The parameters found from the fit of the spectra presented in Fig.5, b are given in Table 5. As is seen from the table, the values of $\xi$, $m$, and $M$ are in good agreement with the expected ones. Thus we can find the values of $\epsilon/\omega$ and of the steady state cycling rate only from the analysis of the neutron multiplicity distribution.

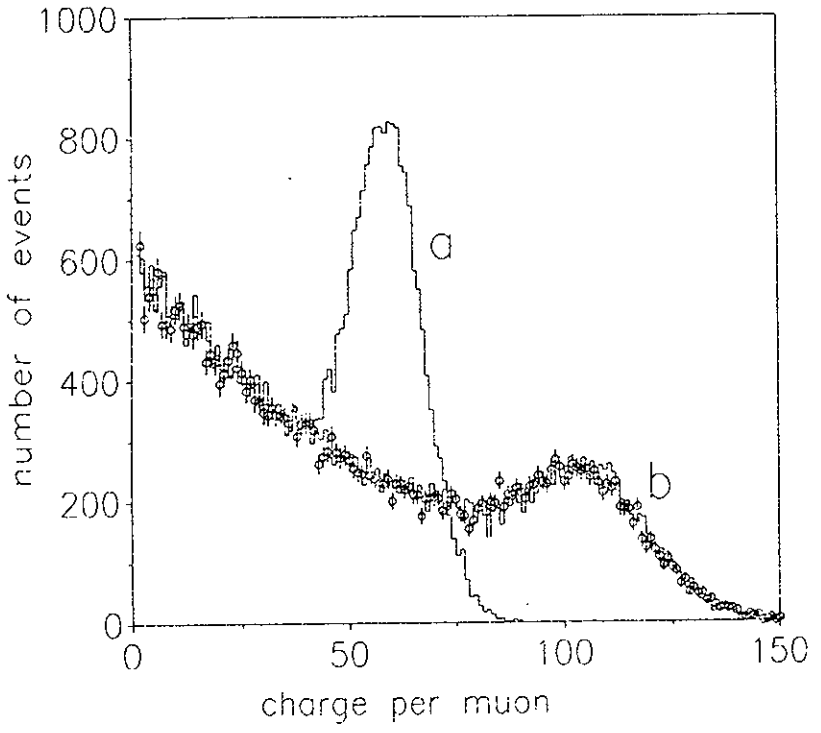


Figure 5: Neutron multiplicity distributions plotted for the observation time $T = 2\,\mu s$ and the values (9). Histograms correspond to an "event mode" with (b) and without (a) taking into account the deceleration stage. Circles are the spectra obtained in a "charge mode".



Table 5. Parameters of the neutron multiplicity distributions (7), (10) calculated for the values (9), $\lambda_c^f = 1000\,\mu s^{-1}$ and for the observation time interval $T = 2\,\mu s$.

| Variant | Parameters | | | | | |
|---|---|---|---|---|---|---|
| | Expected | | | Obtained | | |
| | $\xi$ | m | M | $\xi$ | m | M |
| Fit with formula (6) | 0.0167 | 109.1 | | 0.0166(1) | 108.5(2) | |
| Fit with formula (10) | 0.0167 | 109.1 | 109.1 | 0.0166(3) | 108.4(3) | 113(4) |

**Conclusion.**

It follows from our consideration that in spite of complications in the MCF kinetics caused by the epithermal mu-atom effects, the main parameters of the MCF process can be reliably determined using the novel method [3]. Indeed, the most important characteristics - the neutron yield from the d-t fusion reaction and the probability of muon sticking to helium - can be found from the analysis of the neutron multiplicity distribution (10) without any assumptions about the thermalization stage. The mean of the Gaussian peak in this spectrum determines the steady state cycling rate $\lambda_{ss}$, and a portion of the peak corresponds to the muon sticking probability in the observed cycle $\omega/\epsilon$. Independent charge calibration is desirable but not necessary.

In principle, the value of $\omega/\epsilon$ could be also found from the "$t_e - t_n$" -spectrum. However, in this case the data interpretation is complicated due to influence of the "fast" MCF process whose parameters are very difficult to directly measure at high hydrogen density.

Knowledge of the slopes and amplitudes of exponents corresponding to the steady state for the first detected neutrons and for all detected ones allows in principle the parameters of the "fast" MCF process to be estimated. The most reliable way for this is to directly observe the initial spike in time spectra both of all detected neutrons and of the first detected ones. Exposures with a low tritium concentration in the H/D/T mixture and with the D/T mixture of low density should be carried out for this.

The investigation was supported by the International Science and Technology Center (ISTC).

## References

[1] V.G. Zinov, Muon Cat. Fusion, 7 (1992) 419.

[2] V.V. Filchenkov, Muon Cat. Fusion, 7 (1992) 409.

[3] D.L. Demin et al, Contributed paper to the X-th Int. Symposium on Muon Catalyzed Fusion, Dubna, 19-24 June 1995; to be published in Hyp. Int., 1996.

[4] A.E. Drebushko, V.V. Filchenkov, A.I. Rudenko. Preprint JINR E-15-97-8, Dubna, 1997.

[5] M.P. Faifman, L.I. Ponomarev, Phys. Lett.B **265** (1991) 201.

[6] M.P. Faifman, Contributed paper to the X-th Int. Symposium on Muon Catalyzed Fusion, Dubna, 19-24 June 1995; to be published in Hyp. Int., 1996.

[7] L.I. Menshikov et al, Zh. Exp. Teor. Phys., **92** (1987) 1173. *Sov. Phys.* - JETP, **65**(1987)656.

[8] S.S. Gerstein et al, Zh. Exp. Teor. Phys., **78** (1980) 2099. *Sov. Phys.* - JETP, **51**(1980)1053.

[9] V.V. Filchenkov, L.N. Somov, V.G. Zinov. Nucl. Instr. and Meth., **228** (1984) 174.

[10] V.V. Filchenkov, Preprint JINR, E1-89-57, Dubna, 1989.

[11] V.E. Markushin, in: L.A. Shaller and C. Petitjean (eds.), Muonic Atoms and Molecules, Birkhauser Verlag, Basel, (Switzerland), 1993.

[12] M. Jeitler et al, Muon Cat. Fusion, **5/6** (1991) 217. M. Jeitler, Proceedings of International Workshop on Low Energy Muon Science - LEMS'93, p. 294.

[13] D.V. Balin et al, Contributed paper to the X-th Int. Symposium on Muon Catalyzed Fusion, Dubna, 19-24 June 1995; to be published in Hyp. Int., 1996.

[14] A. Adamchak et al, Atomic Data and Nuclear Data Tables, **62** (1996) 255.

[15] V.P. Dzhelepov et al, Nucl. Instr. and Meth., **A 256** (1988) 634. V.V. Filchenkov, A.D. Konin, A.I. Rudenko, Nucl. Instr. and Meth., **A 294** (1990) 504.

Received by Publishing Department
on January 16, 1997.